Supporting Information for

Volumetric Chemical Imaging by Clearing-Enhanced Stimulated Raman Scattering Microscopy

Mian Wei[a,1], Lingyan Shi[a,1], Yihui Shen[a], Zhilun Zhao[a], Asja Guzman[a], Laura J. Kaufman[a], Lu Wei[a,2,3], Wei Min[a,b,3]

[a]Department of Chemistry, Columbia University, New York, NY 10027;

[b]Kavli Institute for Brain Science, Columbia University, New York, NY 10027

[1]M.W. and L.S. contributed equally to this work.

[2]Present address: Division of Chemistry & Chemical Engineering, California Institute of Technology, Pasadena, CA 91125.

[3]To whom correspondence may be addressed. Email: lwei@caltech.edu or wm2256@columbia.edu.

This file includes:

SI Methods

Cell culture

U-87 MG cells were obtained from ATCC (Manassas, VA) and cultured in Dulbecco's modified Eagle's medium (DMEM, Thermo Fisher) supplemented with 10% fetal bovine serum (Thermo Fisher) in a humidified 5% CO_2 atmosphere at 37°C.

Tumor spheroid sample preparation

Tumor spheroids were formed using Mcf10a-HRas cell lines (kindly provided by Prof. Prives, Columbia University, NY) cultured in 1x DMEM/F-12 medium supplemented with 5% (v/v) horse serum, 1% (v/v) 100x penicillin/ streptomycin/amphotericin B solution (MP Biomedicals, Solon, OH), 0.5 µg/mL hydrocortisone (Sigma-Aldrich), 10 µg/mL insulin (Sigma-Aldrich), 0.1 µg/mL cholera toxin (Sigma-Aldrich), and 20 ng/mL epidermal growth factor (Sigma-Aldrich).

Tumor spheroids were formed with the centrifugation method as previously described (1). In brief, cells were detached through Accutase treatment, brought into suspension in ice-cold culture medium containing 0.2575 mg/ml basement membrane extract (BME) and centrifuged at 4°C for 10 min at 1000-1200 g in a Sorvall desktop centrifuge in ultra-low adhesion U-bottom 96-well culture plates (Thermo Fisher Scientific Nunclon Sphera microplates, Waltham, MA). Culture plates were then transferred to an incubator for 24 h at 37°C with 5% carbon dioxide for tumor spheroid compaction. Tumor spheroids were treated with Cell Recovery Solution (Corning, Corning, NY) for 45-65 min at 4°C prior to embedding in 3D matrices to remove the layer of BME of variable thickness, density, and continuity which would obstruct uniform invasion.

Single tumor spheroids pre-treated with Cell Recovery Solution were placed into composite collagen I/BME biopolymer matrices containing the appropriate concentration of the deuterated lipid probe, each of which could then be gelled around the tumor spheroid. For composite collagen I/BME gels, first 10x DMEM, HEPES buffer, deuterated lipid probe and sodium bicarbonate were mixed. Then, the required amount of BME stock solution (8.9-10 mg/ml) was added to reach the final concentration of 3 mg/ml. The BME replaced a proportion of the ddH_2O that would be added in the equivalent pure collagen I gel. Next the collagen stock solution was added to achieve a concentration of 1 mg/ml, and the solution was brought to pH 7.4 by adding NaOH.

Subsequently, 80 µl of the neutralized collagen/BME solution was transferred to a chamber consisting of an adhesive silicone isolator (Press-to-Seal Invitrogen, 9 mm diameter, 1 mm depth) attached to a coverslip-bottom cell culture dish and a single MTS was added to the biopolymer matrix. The gel chamber was then transferred to the 37°C incubator. After completion of gelation (t = 1 h) the gels were overlaid with 30 µL culture medium containing 20 µM deuterated palmitic acid and surrounded by 500 µL culture medium to prevent drying during extended monitoring. For deuterated palmitic acid solution, palmitic acid-d_{31} (98% D, 366897, Sigma-Aldrich) were reacted with sodium hydroxide (Sigma-Aldrich) above melting point to form 20 mM solution, and then coupled to fatty-acid-free BSA (A7030, Sigma-Aldrich) in about 2:1 molar ratio to make 2 mM stock solution in culture medium. The stock solution was then added to culture medium to a final concentration of 20 µM.

Mouse brain and glioblastoma xenograft sample preparation

The animal experimental protocol (AC-AAAQ0496) was approved by the Institutional Animal Care and Use Committee at Columbia University.

Adult female wild type mice (C57BL/6, 12 weeks old, Jackson Lab) were fully anesthetized using isoflurane, then sacrificed with cervical displacement and immediately perfused with 4% PFA in PBS transcardially. The whole brain was extracted and fixed in 4% PFA in PBS at 4 °C for 24 h. After post-fixation, the brain was sectioned into 1 mm thick coronal slices using a vibratome (VT1000S, Leica).

To obtain glioblastoma xenograft in brain, we performed intracranial implantation of U-87 MG human glioma cells. Briefly, a nude mouse (J:NU, Jackson Lab) was anesthetized and positioned in a stereotaxic instrument (David Kopf Instruments), and then a small section (2 mm in diameter) of the skull was ground with a dental drill until it became soft and translucent. Subsequently, we injected 1.5×10^5 U87-MG cells (in 3 μL) into the frontal region of the cerebral cortex over the course of 5 minutes using a glass capillary. After the implantation, mouse head skin was then closed with SILK sutures (Harvard Apparatus). 2~3 weeks later, mice bearing glioblastoma were anesthetized, sacrificed, fixed, and sliced for clearing and SRS imaging.

For subcutaneous glioblastoma xenograft, we injected subcutaneously 1×10^7 U87-MG cells into the lower flank of nude mice. After ~10 days, tumor bearing mice were anesthetized, sacrificed, fixed, and sliced for clearing and SRS imaging.

Deuterium oxide (D_2O) labeling of glioblastoma xenograft

D_2O labeling of glioblastoma xenograft was performed as previously described (2). Briefly, after intracranial implantation of U87-MG cells in nude mice, tumors were allowed to grow for 10 days. Tumor-bearing mice were then given 25% D_2O as drinking water for 15 days before being sacrificed and fixed. After post-fixation, tumor xenograft samples were sectioned into 1 mm thick coronal slices for clearing and SRS imaging and sectioned into 40 μm coronal slices for immunolabeling and correlative immunofluorescence and SRS imaging.

Tissue clearing

For tumor spheroid samples, the clearing solution (8 M urea) was prepared by adding 16 mL deionized water to the product vial (U4883, Sigma-Aldrich). Tumor spheroid samples were immersed in the clearing solution for more than four days at room temperature and were then mounted in the clearing solution for stimulated Raman scattering microscopy.

For mouse brain and glioblastoma xenograft samples, the clearing solution (8 M urea and 0.2% Triton X-100) was prepared by diluting Triton X-100 (H5142, Promega) in 8 M urea (8 M after adding 16 mL deionized water, U4883, Sigma-Aldrich) to a final concentration of 0.2%. Samples

were immersed in the clearing solution for more than four days at room temperature and were then mounted in the clearing solution for Raman spectroscopy or SRS microscopy.

For samples that underwent 15% treatment (Fig. S4), brain slices were immersed in the solution of 8 M urea and 15% Triton X-100 for 4 days and then in the clearing solution of 8 M urea and 0.2% Triton X-100 for four days at room temperature. After that, the samples were mounted in the clearing solution (8 M urea and 0.2% Triton X-100) for Raman spectroscopy or SRS microscopy.

For samples that underwent 3DISCO treatment (Fig. S5), brain slices were processed using 3DISCO procedures as previously reported (3). After that, the samples were immersed in PBS for four days at room temperature and were then mounted in PBS for Raman spectroscopy or SRS microscopy.

Immunolabeling of glioblastoma xenograft

After post-fixation, D_2O labeled glioblastoma xenografts was sectioned into 40 μm coronal slices using a vibratome (VT1000S, Leica). Tumor slices were washed three times for 5 min each using PBS. Samples were then permeabilized with 0.5% Triton X-100 in PBS for 10 min and washed twice with 10% goat serum/1% BSA/0.3 M glycine solution. After that samples were incubated with a human-specific anti-vimentin antibody (mouse monoclonal [V9] to vimentin, ab8069, Abcam) at 1:200 dilution in 3% BSA overnight at 4 °C. Samples were washed twice for 5 min each time using PBS and washed once using 10% goat serum. Samples were then blocked with 10% goat serum for 30 min. After that samples were incubated with goat anti-mouse IgG conjugated with Alexa Fluor 647 (A21236, Invitrogen) at 1:500 dilution in 10% goat serum overnight at 4 °C. Samples were then washed with PBS before imaging.

Spontaneous Raman spectroscopy

Spontaneous Raman spectra were acquired using an upright confocal Raman spectrometer (Xplora, HORIBA Jobin Yvon). Samples were illuminated by 532 nm (25 mW) laser through a 50× objective (air, NA 0.75, MPlan N, Olympus). The acquisition time was 10 s with 5× accumulation. For the spectra of tissue samples, at least three different regions were randomly chosen and their spectra were averaged.

Stimulated Raman scattering (SRS) microscopy

An integrated laser (picoEMERALD with custom modification, Applied Physics and Electronics, Inc.) was used as a light source for both pump and Stokes beams. Briefly, picoEMERALD provided an output pulse train at 1064 nm with 6-ps pulse width and 80-MHz repetition rate, which served as the Stokes beam. The frequency-doubled beam at 532 nm was used to synchronously seed a picosecond optical parametric oscillator (OPO) to produce a mode-locked pulse train (the idler beam of the OPO was blocked with an interferometric filter) with 5-6-ps pulse width. The

wavelength of the OPO was tunable from 720 nm to 990 nm, which served as the pump beam. The intensity of the 1,064 nm Stokes beam was modulated sinusoidally by a built-in electro-optic modulator (EOM) at 8 MHz with a modulation depth of more than 95%. The pump beam was spatially overlapped with the Stokes beam with a dichroic mirror inside picoEMERALD. The temporal overlap between pump and Stokes pulse trains was ensured with a built-in delay stage and optimized by the SRS signal of deuterium oxide (99.9 at% D, 151882 ALDRICH).

Pump and Stokes beams were coupled into an inverted laser-scanning microscope (FV1200MPE, Olympus) optimized for near-infrared throughput. A 25× water objective (XLPlan N, 1.05 numerical aperture (NA), MP, Olympus) with high near-infrared transmission and large field of view was used for measurements of all samples. The pump/Stokes beam size was matched to fill the back-aperture of the corresponding objectives for imaging. The forward-going pump and Stokes beams after passing through the samples were collected in transmission with a high-NA condenser lens (oil immersion, 1.4 NA, Olympus), which was aligned following Köhler illumination. A telescope was then used to image the scanning mirrors onto a large-area (10 mm × 10 mm) Si photodiode (FDS1010, Thorlabs) to descan beam motion during laser scanning. The photodiode was reverse-biased by 64 V from a DC power supply to increase the saturation threshold and the response bandwidth. A high-optical-density bandpass filter (890/220 CARS, Chroma Technology) was used to block the Stokes beam completely and transmit the pump beam only. The output current of the photodiode was electronically pre-filtered by an 8-MHz bandpass filter (KR 2724, KR electronics) to suppress the 80-MHz laser pulsing and the low-frequency contribution due to laser scanning across the scattering sample. It was then fed into a radio-frequency lock-in amplifier (HF2LI, Zurich instrument), terminated with 50 Ω to demodulate the stimulated Raman loss signal experienced by the pump beam. The in-phase X-output of the lock-in amplifier was fed back into the analogue interface box (FV10-ANALOGUE) of the microscope.

All laser powers were measured after the objective lens. The pump laser power was 125 mW and the Stokes laser power was 175 mW. For the imaging of tumor spheroids, the pixel dwell time was 8 μs (1.261 s per 320 × 320 frame), the time constant of the lock-in amplifier was 5 μs, and z series were captured at 2 μm steps. For the imaging of the mouse brain, tumors, and embryos, the pixel dwell time was 4 μs (1.644 s per 512 × 512 frame), the time constant of the lock-in amplifier was 3 μs, and z series were captured at 4 μm steps. For metabolic volumetric chemical imaging of glioblastoma xenograft, the pixel dwell time was 40 μs (11.297 s per 512 × 512 frame), the time constant of the lock-in amplifier was 30 μs, and z series were captured at 4 μm steps. The wavelength of the Stokes laser was 1064 nm and the wavelengths for the pump laser were 810.5 nm (2940 cm^{-1}, mainly protein CH_3), 816.7 nm (2845 cm^{-1}, mainly lipid CH_2), 869.0 nm (2109 cm^{-1}, C-D for newly synthesized lipids from d-PA), 875.0 nm (2030 cm^{-1}, off-resonance background for newly synthesized lipids from d-PA), 863.3 nm (2185 cm^{-1}, C-D for mainly newly synthesized proteins from D_2O), 867.2 nm (2135 cm^{-1}, C-D for mainly newly synthesized lipids from D_2O), and 885.0 nm (1901 cm^{-1}, off-resonance background for newly synthesized proteins and lipids from D_2O).

Multispectral SRS imaging

The pump laser power was 125 mW and the Stokes laser power was 175 mW. The pixel dwell time was 4 μs (1.644 s per 512 × 512 frame), the time constant of the lock-in amplifier was 3 μs, and z series were captured at 8 μm steps. The wavelength of the Stokes laser was 1064 nm. The wavelengths for the pump laser were tuned to 800.7 nm (3091 cm^{-1}), 802.5 nm (3063 cm^{-1}), 804.4 nm (3033 cm^{-1}), 806.2 nm (3005 cm^{-1}), 808.1 nm (2976 cm^{-1}), 809.9 nm (2949 cm^{-1}), 810.5 nm (2940 cm^{-1}), 811.7 nm (2921 cm^{-1}), 813.6 nm (2893 cm^{-1}), 815.4 nm (2865 cm^{-1}), 816.7 nm (2845 cm^{-1}), 817.3 nm (2837 cm^{-1}), and 819.1 nm (2810 cm^{-1}) sequentially for multispectral imaging. A whole z-stack image was taken at each wavelength before tuning.

Correlative imaging of immunofluorescence and SRS

Confocal fluorescence imaging was performed on the inverted laser-scanning microscope (FV1200MPE, Olympus) with a 633-nm continuous-wave laser. After fluorescence imaging, we switched to SRS imaging mode and collected label-free SRS and DO-SRS signals with the Stokes laser (1064 nm, 175 mW) and the pump laser (810.5 nm, 816.7 nm, 863.3 nm, 867.2 nm, and 885 nm, 125 mW).

Correlative two-photon fluorescence and SRS imaging

Correlative two-photon fluorescence and SRS imaging was performed with the integrated laser (picoEMERALD with custom modification, Applied Physics and Electronics, Inc.) and the inverted laser-scanning microscope (FV1200MPE, Olympus). We first tuned the pump laser to 810.5 nm (125 mW) and used it to collect two-photon excited autofluorescence from the samples. We then switched to SRS imaging mode and collected label-free SRS signals with the Stokes laser (1064 nm, 175 mW) and the pump laser (810.5 nm and 816.7 nm, 125 mW).

Correlative second-harmonic generation and SRS imaging

Correlative second-harmonic generation and SRS imaging was performed with the integrated laser (picoEMERALD with custom modification, Applied Physics and Electronics, Inc.) and the inverted laser-scanning microscope (FV1200MPE, Olympus). We first used the Stokes laser (1064 nm, 125 mW) to collect second-harmonic generation signals from the samples. We then switched to SRS imaging mode and collected label-free SRS signals with the Stokes laser (1064 nm, 175 mW) and the pump laser (810.5 nm and 816.7 nm, 125 mW).

CH_2 and CH_3 linear combination algorithm

In order to obtain total lipid and total protein signals, we adapted a previously reported spectral linear combination algorithm (4). Briefly, we acquired the SRS signals from two wavelengths bearing features of lipids and proteins and the total amounts of lipids and proteins can be determined by a linear combination of the signals at those two wavelengths, with coefficients

obtained by pure substances and then fine-tuned and optimized by actual unmixed images. Here, signals at 2845 cm^{-1} and 2940 cm^{-1} were measured to perform the spectral unmixing:

Protein: $CH_P = I_{2940} - I_{2845}$

Lipid: $CH_L = 5 \cdot I_{2845} - 0.4 \cdot I_{2940}$

where I_{2845} and I_{2940} are SRS signal intensities at 2845 and 2940 cm^{-1}, respectively.

CD_L and CD_P unmixing algorithm

SRS images at 2185 and 2135 cm^{-1} were corrected by subtracting off-resonance images at 1901 cm^{-1}. CD_L and CD_P signals were then unmixed using the equations (2):

$CD_L = 1.25 \cdot I_{2135} - 0.50 \cdot I_{2185}$

$CD_P = 1.25 \cdot I_{2185} - 0.64 \cdot I_{2135}$

where I_{2135} and I_{2185} are signal intensities of corrected SRS images at 2135 and 2185 cm^{-1}, respectively.

Three dimensional reconstruction

Raw images were unmixed into two channels—total proteins and total lipids. For tumor spheroids, an additional channel of newly synthesized lipids was obtained by subtracting the images acquired at 869.0 nm pump laser by that at 875.0 nm pump laser. For metabolic imaging of glioblastoma xenograft, raw images were corrected by subtracting off-resonance background and then unmixed into two channels of newly synthesized proteins (CD_P) and lipids (CD_L). A median filter was applied to the unmixed images for noise reduction. A Fiji plugin (5) was then applied to the images for attenuation correction. The opening radius was set to 0.5 for 512 × 512 frames or 0.2 for 320 × 320 frames. After correction, the images were volume-rendered in the mode of maximal intensity projection using Imaris (Bitplane).

Quantification of imaging depth

The imaging depths were determined based on z-series images at 2940 cm^{-1} for label-free images. The signal-to-background ratios of the raw images were quantified at different z depths using Fiji (6). Specifically, for an image acquired at a specific depth, we drew several lines on the image with each line across multiple cells, plotted the intensity profiles for individual lines, calculated the signal-to-background ratio for each line (using minimal intensity as the background and maximal intensity as the sum of the background and the signal), and averaged the signal-to-background ratios of these lines as the signal-to-background ratio of the image. The imaging depth was determined when the signal-to-background ratio decreased to less than 0.5 at this specific depth.

Image registration between images before and after clearing

To confirm that the process of tissue clearing preserved tissue and cellular structures, we imaged the same region of the tissue before and after clearing and then registered and compared the two images in both total protein and total lipid channels. First, the raw images were unmixed into total protein and total lipid channels. Then the unmixed images before and after clearing were registered using a Fiji plugin TrakEM2 (7). Four images—total protein before clearing, total protein after clearing, total lipid before clearing, and total lipid after clearing—are loaded into four different layers in TrakEM2. The image of total proteins after clearing was aligned to that of total proteins before clearing using the mode of least squares and similarity transformation. After that, the image of total lipids before clearing was aligned to that of total proteins before clearing and the image of total lipids after clearing was aligned to that of total proteins after clearing, manually using the outer edges of the images. After registration, the protein/lipid ratios were measured and compared at the same regions before and after clearing. The fold of expansion after tissue clearing was calculated by dividing the length of the edge before clearing by that after clearing.

Ratiometric imaging analysis

SRS images at 2940 and 2845 cm^{-1} were acquired by point scanning (pixel size: 1.988 μm) and stitched into large-area images using Olympus Fluoview software. Ratiometric imaging analysis was performed using ImageJ (8). Raw images were unmixed into protein and lipid channels and then corrected with background subtraction. The protein/lipid ratiometric image was calculated as the background-corrected protein image divided by the background-corrected lipid image. Artifacts outside the brain sample region were removed using a mask image generated from the protein image. For each image at a specific depth, mean protein/lipid ratios were measured for three regions of interests in the tumor tissue and three regions of interests in the normal tissue. Protein/lipid ratios were plotted as a function of imaging depths. CD_P/CD_L ratiometric images were produced similarly.

Volumetric phasor analysis

The multispectral SRS imaging data were transformed to a phasor plot as described previously (9) using custom-written Matlab scripts. Each voxel in the 4D (x-y-z-λ) dataset was transformed to a phasor point on a 2D phasor plot using the following equations of Fourier transform:

$$u = \frac{\sum_{n=1}^{N} S(\lambda_n)\cos(2\pi n/N)}{\sum_{n=1}^{N} S(\lambda_n)}, v = \frac{\sum_{n=1}^{N} S(\lambda_n)\sin(2\pi n/N)}{\sum_{n=1}^{N} S(\lambda_n)}$$

where $S(\lambda_1)$, …, $S(\lambda_N)$ is the SRS spectrum at individual voxels for N spectral points (λ_1, …, λ_N). As 13 wavenumbers were sampled in multispectral SRS imaging, N = 13. The whole 4D dataset is projected onto a 2D Fourier space: each voxel in the real space (x,y,z) corresponds to a point in

the phasor space (u,v). Multiple regions that contained only one type of species (such as axon, vasculature, or nuclei) were cropped manually (as the procedure in Reference (9)) based on structural features in the unmixed protein and lipid images and then transformed to a reference phasor plot. According to the positions of individual species on the reference phasor plot, the phasor plot of the whole volumetric multispectral image was divided into several clusters representing these species. Each cluster on the phasor plot was projected to a binary volumetric image stack using custom-written Matlab scripts. Volume-rendered binary images were generated using Imaris and evaluated for the segmentation results. Several rounds of clustering, projection, and evaluation were conducted to achieve good segmentation. Volume fractions of individual species were calculated as the sum of all the voxels divided by the total number of voxels in the binary volumetric image stack. The total number of voxels in the dense tumor or the normal tissue was determined by delineating tumor margins using the raw image at 2940 cm^{-1} and dividing all the voxels into tumor or normal group accordingly. Single-cell spectra were generated by cropping regions of individual cells and plotting the signal intensity at different wavenumbers.

Quantification of minimal distances

Quantification of minimal distances was conducted using Volocity (PerkinElmer). For noise reduction, a median filter was applied to binary image stacks of tumor cells, vasculature, and axons. Individual tumor cells, blood vessels, and axons were identified using "Find object" with intensity thresholds and volume thresholds. Distances from the centroids of tumor cells to the edges of blood vessels/axons were quantified using "Measure distance". The results of distances were exported and plotted as histograms of minimal distances.

Quantification of metabolic activities in vasculature and clusters of newly synthesized lipids

Quantification of metabolic activities in vasculature and clusters of newly synthesized lipids was conducted using Volocity (PerkinElmer) and ImageJ (8). First, tumor and normal tissues were segmented using "Find object" with intensity thresholds in the CD_P channel. A mask of vasculature was generated using the Tubeness filter (ImageJ) in the CH_P channel. Vasculature in tumor tissue was identified using "Intersect" between the mask of vasculature and the segmented tumor tissues. Vasculature in normal tissues was identified using "Intersect" between the mask of vasculature and the segmented normal tissues. CD_P, CD_L, CH_P, and CH_L intensities were measured for each identified blood vessels in tumor and normal tissues. Clusters of newly synthesized lipids were segmented using "Find object" with intensity thresholds and volume thresholds in the CD_L channel. Clusters in tumor tissues were identified using "Intersect" with the segmented tumor tissues. Clusters in normal tissues were identified using "Intersect" with the segmented normal tissues. Volume and CD_L intensities were measured for each identified clusters in tumor and normal tissues.

1. Ivascu A, Kubbies M (2006) Rapid generation of single-tumor spheroids for high-throughput cell function and toxicity analysis. *J Biomol Screen* 11:922-932.
2. Shi L*, et al.* (2018) Optical imaging of metabolic dynamics in animals. *Nat Commun* 9:2995.
3. Erturk A*, et al.* (2012) Three-dimensional imaging of solvent-cleared organs using 3DISCO. *Nat Protoc* 7:1983-1995.
4. Yu ZL, et al. (2012) Label-free chemical imaging in vivo: three-dimensional non-invasive microscopic observation of amphioxus notochord through stimulated Raman scattering (SRS). *Chem Sci* 3:2646-2654.
5. Biot E, et al. (2008) A new filter for spot extraction in N-dimensional biological imaging. *ISBI'08: From Nano to Macro* 975-978.
6. Schindelin J*, et al.* (2012) Fiji: an open-source platform for biological-image analysis. *Nat Methods* 9:676-682.
7. Cardona A, et al. (2012) TrakEM2 Software for Neural Circuit Reconstruction. *Plos One* 7:e38011.
8. Schneider CA, Rasband WS, & Eliceiri KW (2012) NIH Image to ImageJ: 25 years of image analysis. *Nat Methods* 9:671-675.
9. Fu D, Xie XS (2014) Reliable cell segmentation based on spectral phasor analysis of hyperspectral stimulated Raman scattering imaging data. *Anal Chem* 86:4115-4119.
10. Orringer DA*, et al.* (2017) Rapid intraoperative histology of unprocessed surgical specimens via fibre-laser-based stimulated Raman scattering microscopy. *Nat Biomed Eng* 1:0027.

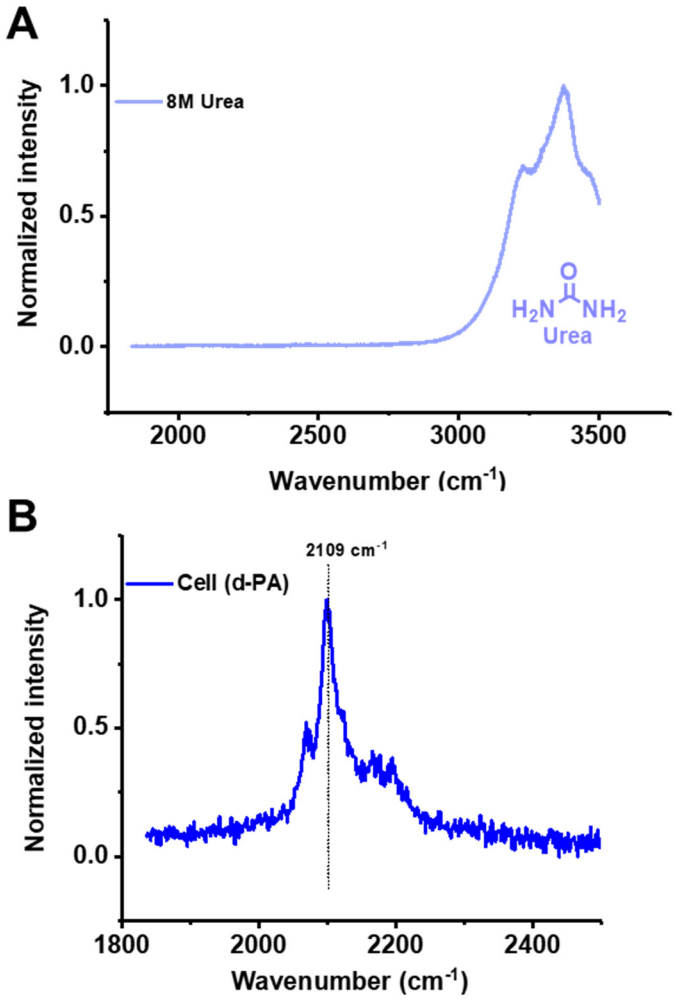

Fig. S1. Spontaneous Raman spectra. (*A*) Spontaneous Raman spectra of 8 M urea solution. (*B*) Spontaneous Raman spectra of cells treated with d-PA.

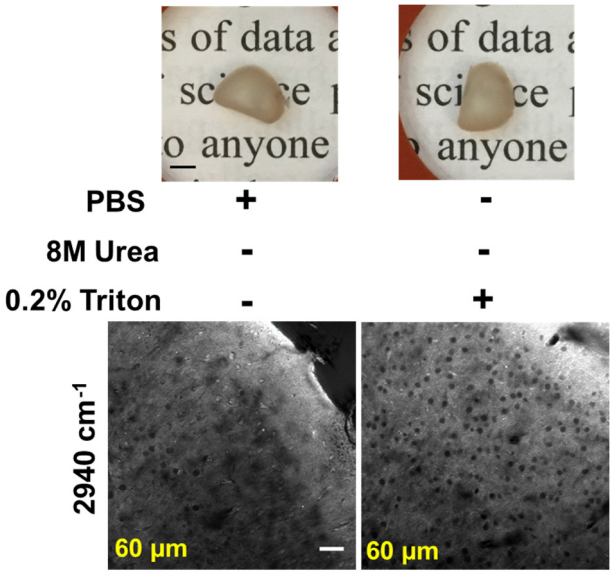

Fig. S2. 0.2% Triton X-100 alone cannot clear tissue. Photos and SRS images of 1 mm-thick brain slices in PBS and those treated with 0.2% Triton X-100 alone. Scale bars: 1mm for photos (*Upper*), 50 µm for SRS images (*Lower*).

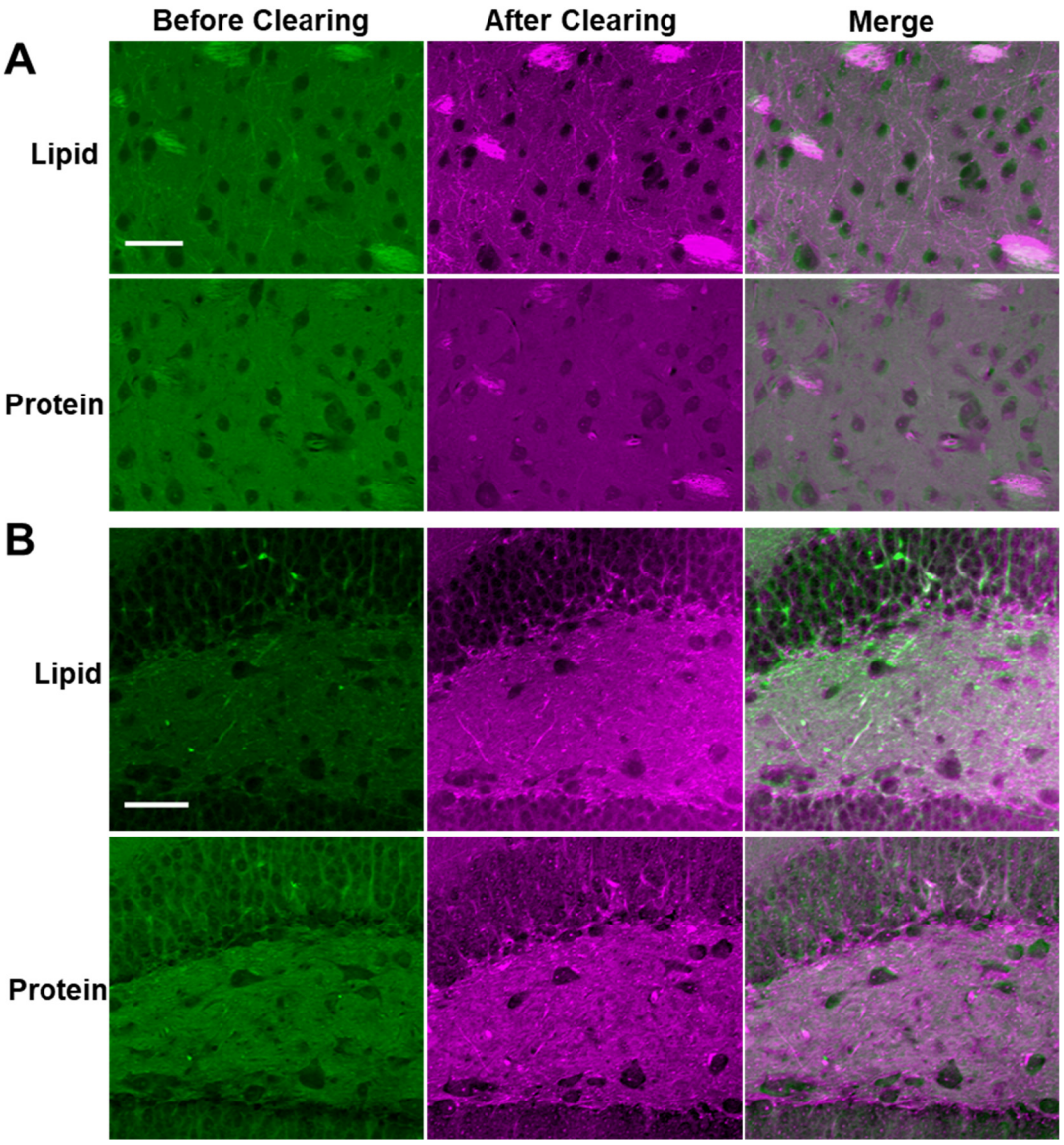

Fig. S3. Preservation of tissue structures after tissue clearing. (*A* and *B*) SRS images of regions in the white matter (*A*) and the hippocampus (*B*). Top row, lipid channel; bottom row, protein channel. Left column, before clearing; middle column, after clearing; right column, merge. Scale bars, 50 μm.

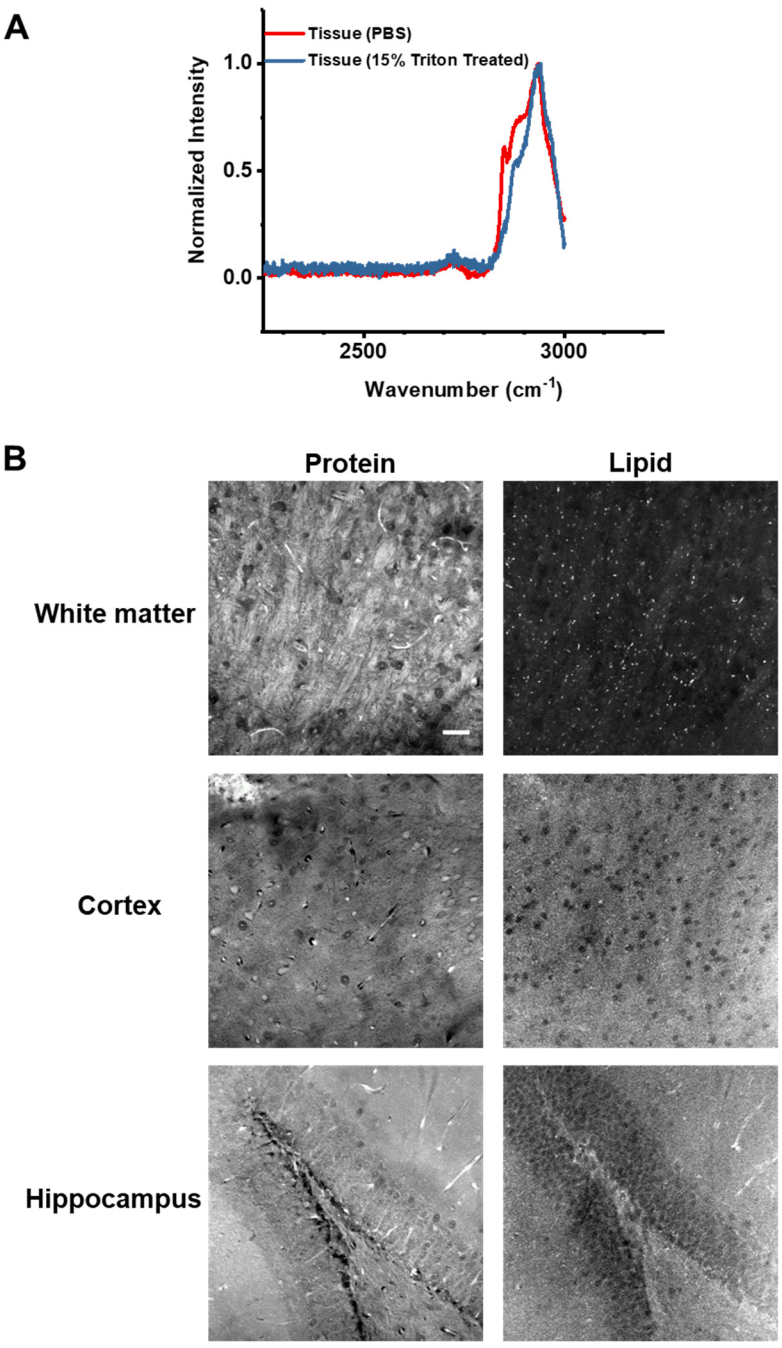

Fig. S4. Treatment of 15% Triton X-100 disrupts lipid structures. (*A*) Raman spectra of mouse brain slices in PBS and those treated with 8 M urea and 15% Triton X-100 for 4 days and then restored with 8 M urea and 0.2% Triton X-100 for 4 days. (*B*) SRS images of the white matter, the cerebral cortex, and the hippocampus from the restored tissue. Left column, protein; right column, lipid. Scale bar, 50 μm.

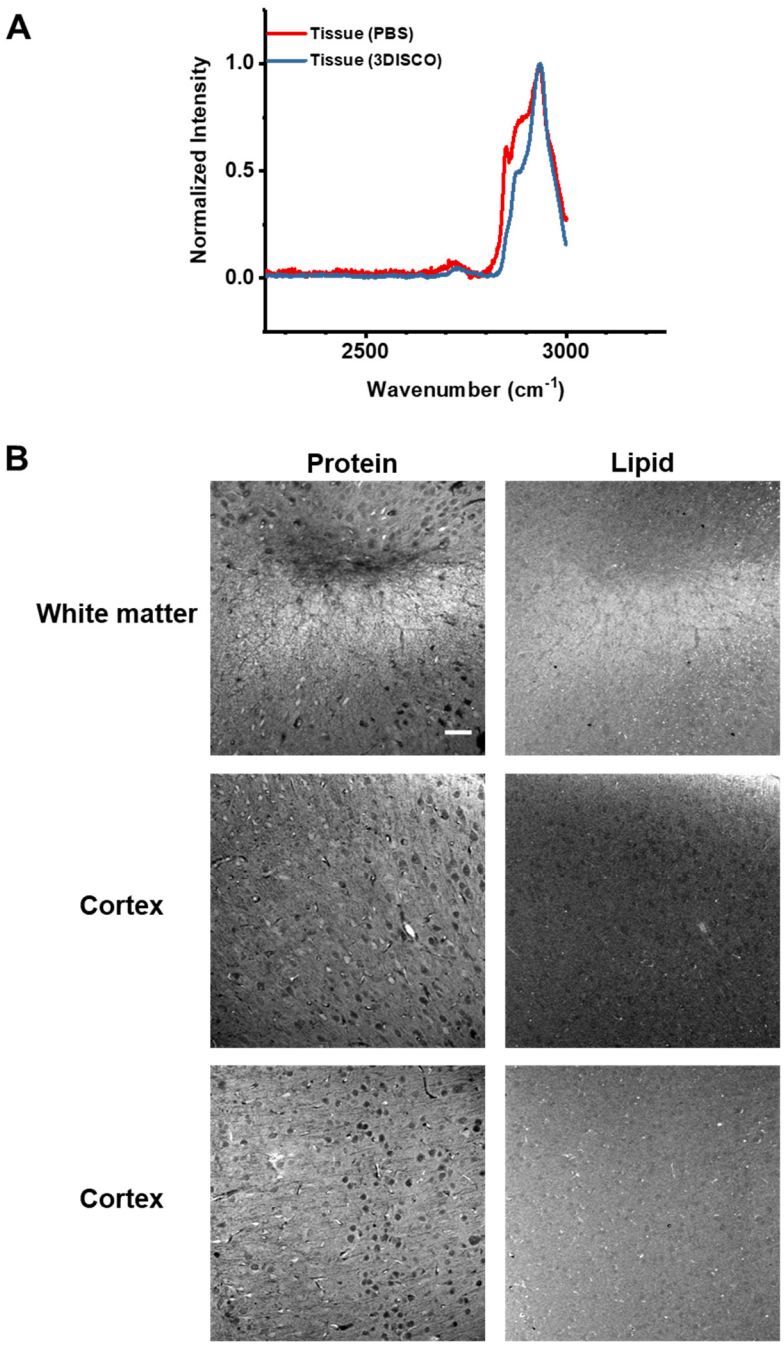

Fig. S5. 3DISCO disrupts lipid structures. (*A*) Raman spectra of mouse brain slices in PBS and those treated with the 3DISCO method and then restored with PBS for 4 days. (*B*) SRS images of the white matter and the cerebral cortex from the restored tissue. Left column, protein; right column, lipid. Scale bar, 50 μm.

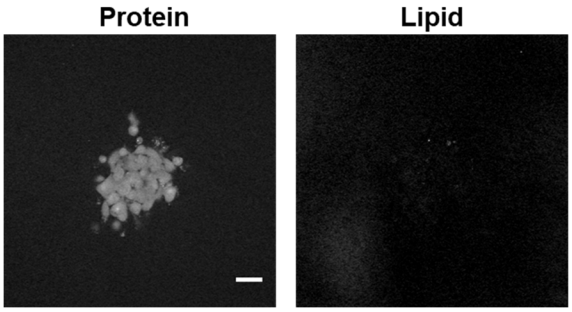

Fig. S6. 0.2% Triton X-100 removes lipids from multicellular tumor spheroids. SRS images of the multicellular tumor spheroid treated with 8 M urea and 0.2% Triton X-100. Left, protein; right, lipid. Scale bar, 50 μm.

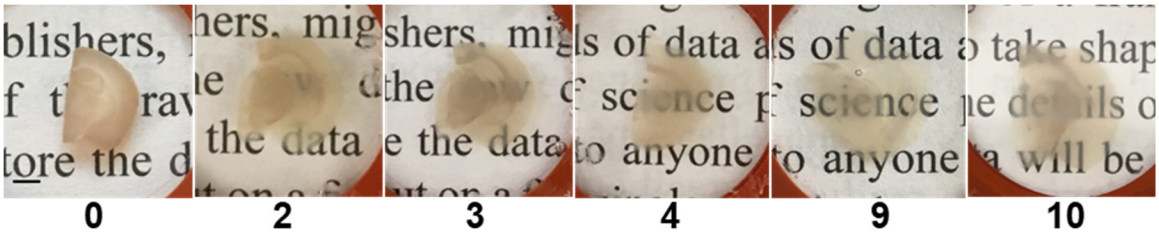

Fig. S7. Optimal incubation time for tissue clearing for 1 mm brain tissues in 8 M urea and 0.2% triton X-100. Photos of the brain slices after different days of tissue clearing treatment. Scale bar, 2 mm.

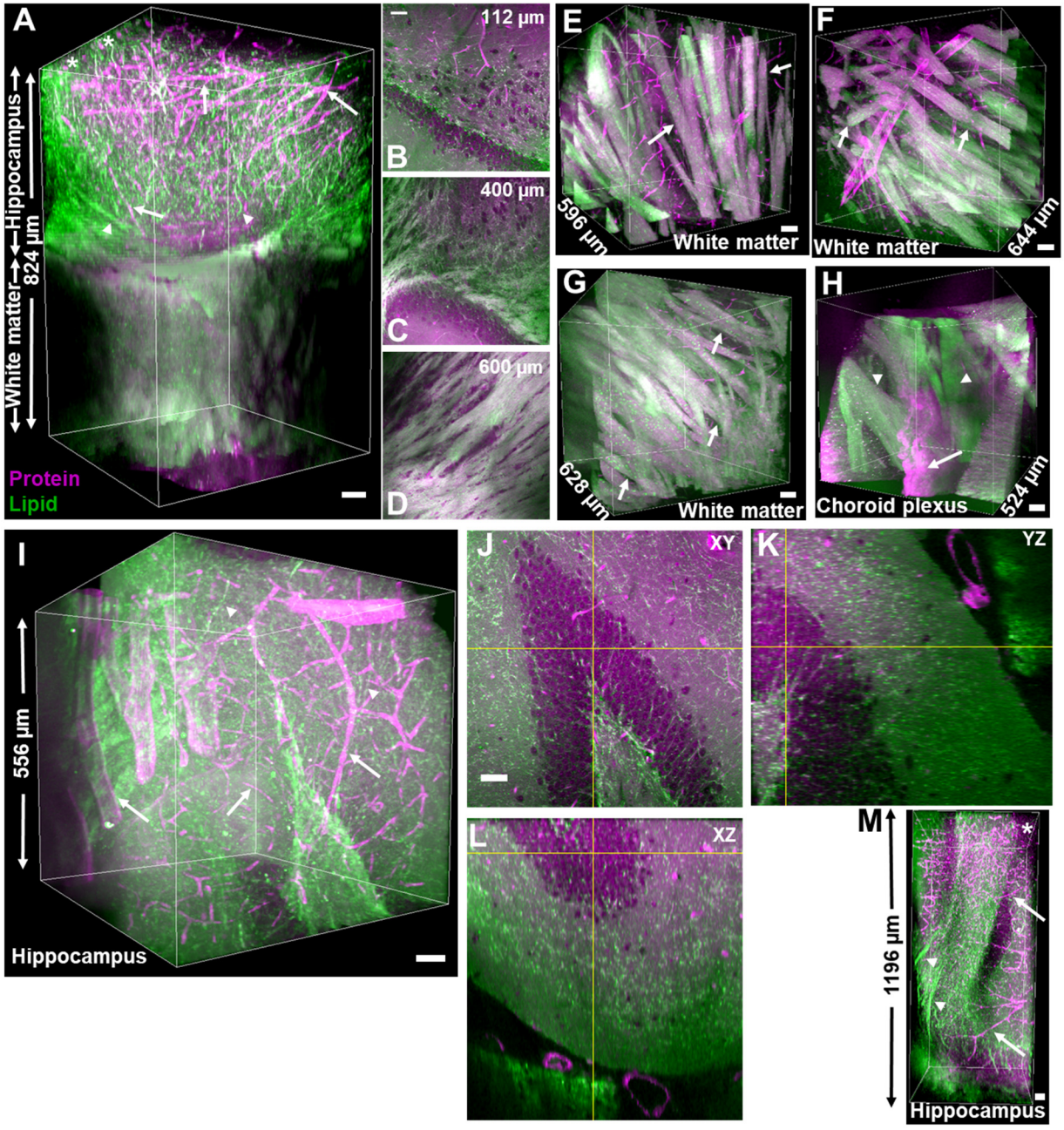

Fig. S8. Volumetric chemical imaging of various regions in mouse brains. (*A*) 3D reconstruction of the hippocampus and white matter. Arrows indicate vasculatures, arrowheads indicate axons, and stars indicate cell bodies. (*B-D*) 2D images at increasing depths of *A*. (*E-G*) 3D reconstruction of the white matter. Arrows indicate nerve tracts. (*H*) 3D reconstruction of the choroid plexus. Arrows indicate the choroid plexus and arrowheads indicate nerve tracts. (*I*) 3D reconstruction of the hippocampus. Arrows indicate vasculatures and arrowheads indicate axons. (*J-L*) orthogonal views of the hippocampus in *I*. *J*, xy view; *K*, yz view; *L*, xz view. (*M*) 3D reconstruction of the hippocampus. Arrows indicate vasculatures, arrowheads indicate axons, and stars indicate cell bodies. Scale bars, 50 µm.

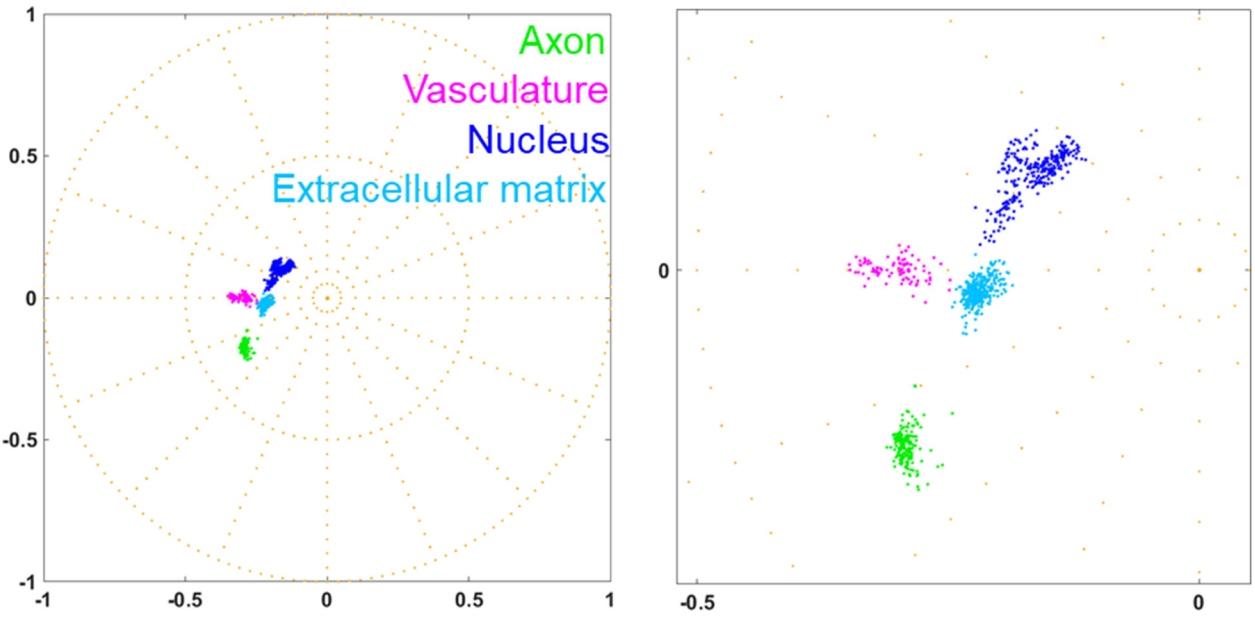

Fig. S9. Reference phasor plot of mouse brain tissues. The right plot is a zoom-in view of the left plot.

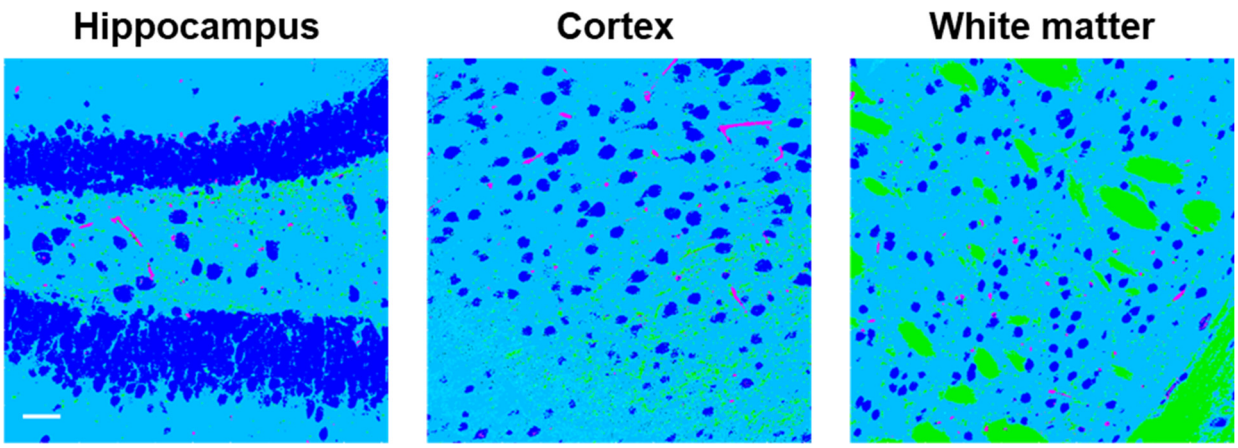

Fig. S10. Single-plane images of segmentation by volumetric phasor analysis in different mouse brain regions. The color code is the same as that in Fig. 3 *B-D*: green, axon; blue, nucleus; magenta, vasculature; purple, water; cyan, other components. Scale bar: 50 μm.

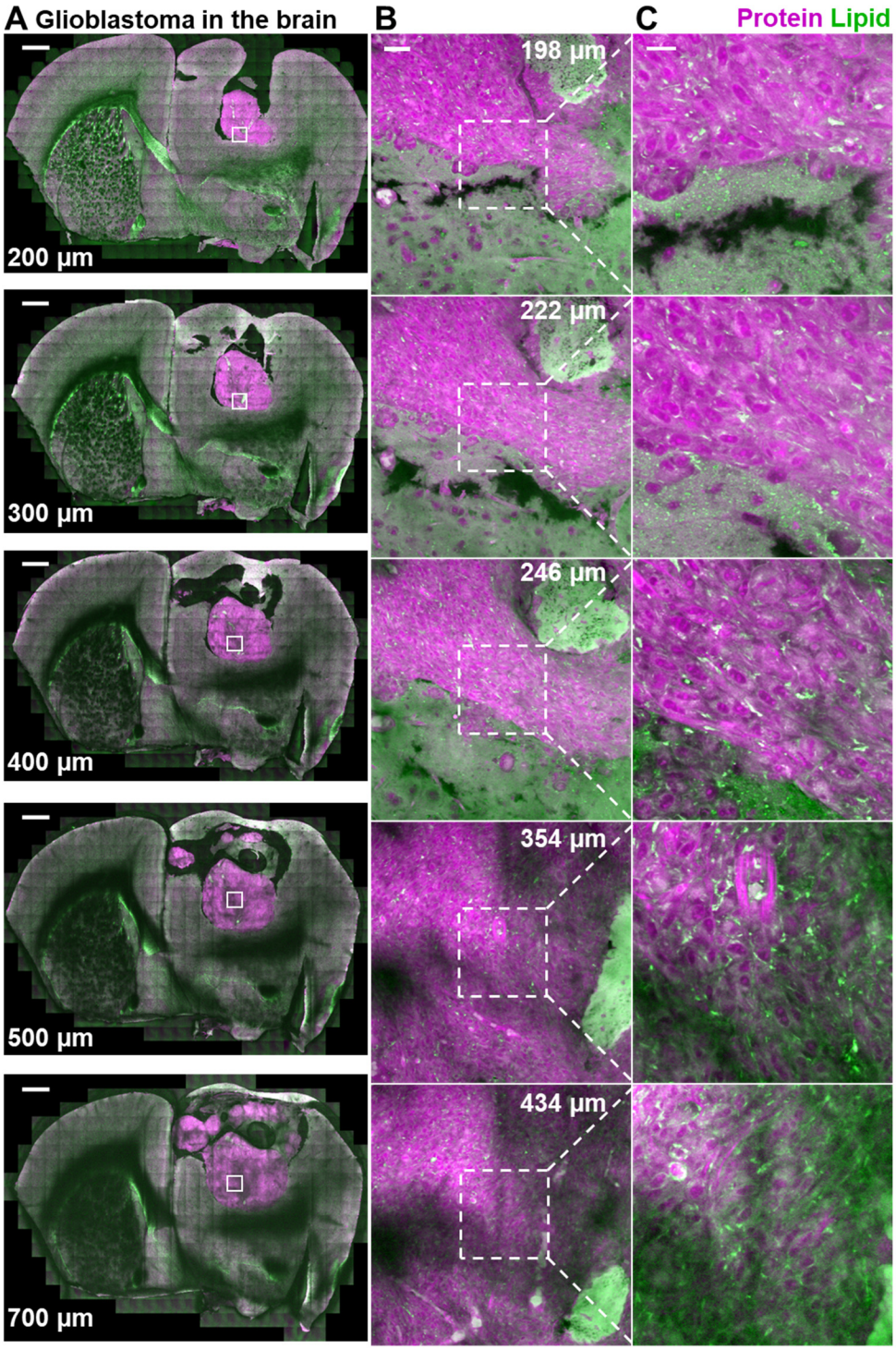

Fig. S11. Volumetric chemical imaging of the glioblastoma in the brain. (*A*) 2D images of the tumor in the whole coronal slice at increasing imaging depths (same as Fig. 4*A*). (*B*) 2D images of the white-box region in *A* at increasing imaging depths. (*C*) Zoom-in images of the white dash-line region in *B*. Imaging depths of *A* are labeled at the bottom left. Imaging depths of *B and C* are labeled at the top regions of *B*. Protein, magenta. Lipid, green. Scale bars: 1mm in *A*, 50 µm in *B*, 20 µm in *C*.

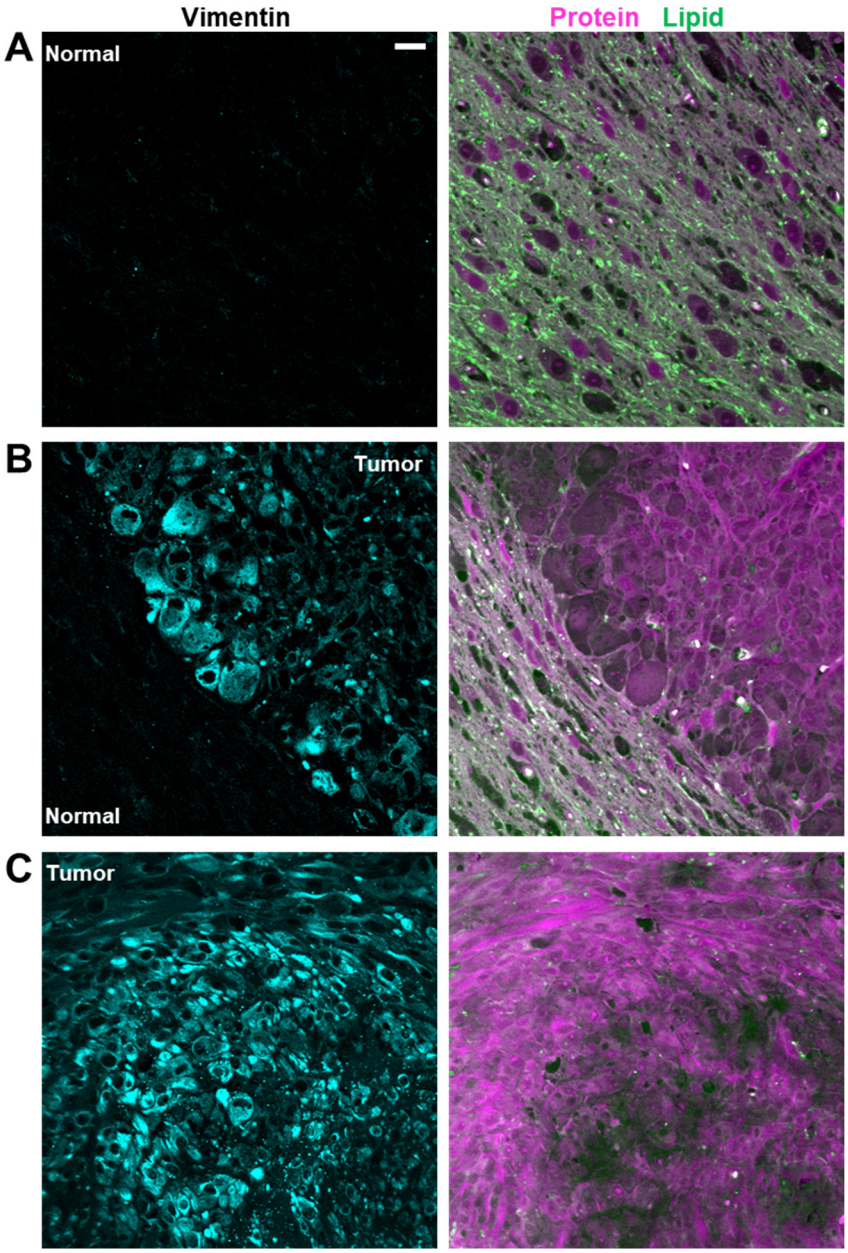

Fig. S12. Immunolabeling with a human-specific vimentin antibody confirms the tumor margin. Correlative images of immunofluorescence and SRS in the regions of (*A*) normal tissue, (*B*) tumor margin, and (*C*) tumor. Scale bar: 20 μm.

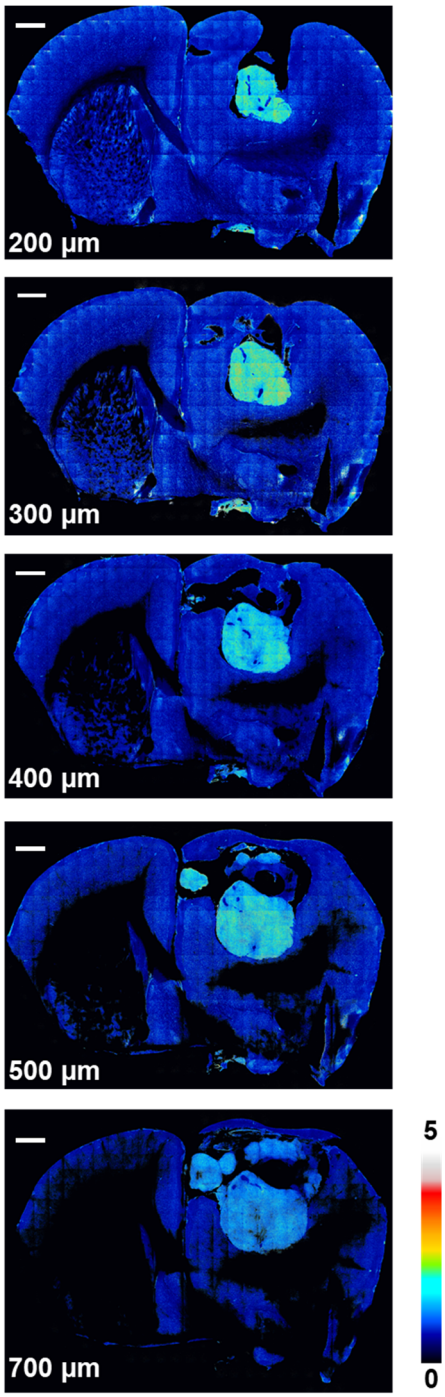

Fig. S13. Protein/lipid ratiometric mapping of glioblastoma in mouse brain. Ratiometric images of the tumor in the whole coronal slice at increasing imaging depths.

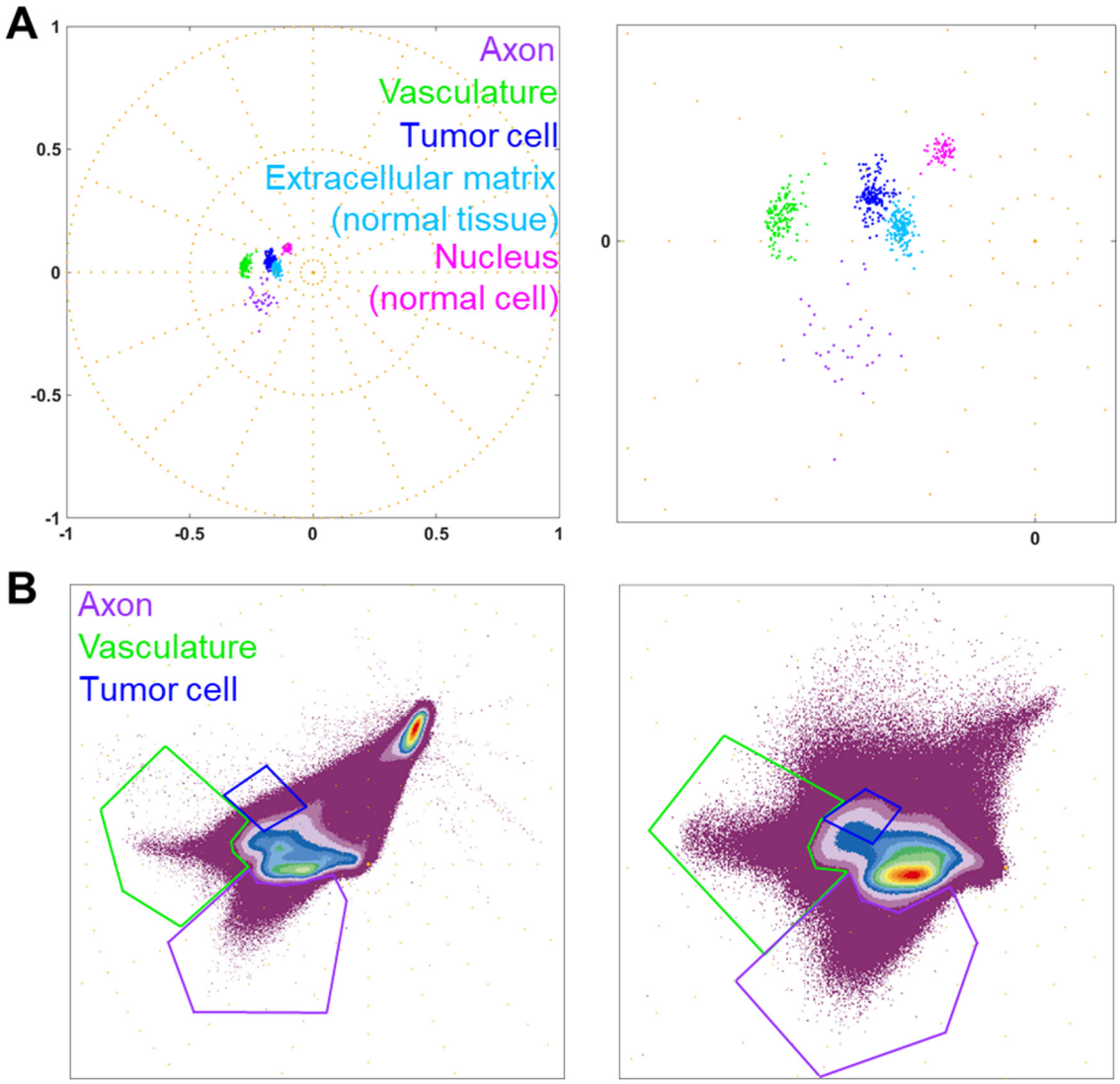

Fig. S14. Phasor plots of brain glioblastoma tissues. (*A*) Reference phasor plots of brain glioblastoma tissues. The right plot is a zoom-in view of the left plot. (*B*) Phasor plots of the brain glioblastoma tissues in Fig. 6*A*.

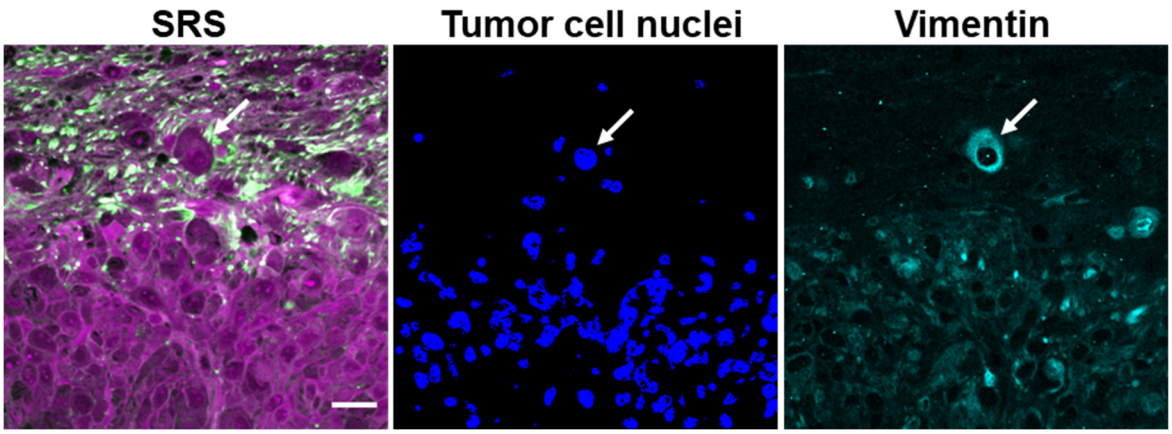

Fig. S15. Immunolabeling with a human-specific vimentin antibody confirms tumor margins and infiltrating tumor cells identified by volumetric phasor analysis. The arrow indicates an infiltrating tumor cell. Left, SRS image. Middle, tumor cell nuclei identified by volumetric phasor analysis. Right, immunofluorescence image of vimentin. Scale bar: 20 μm.

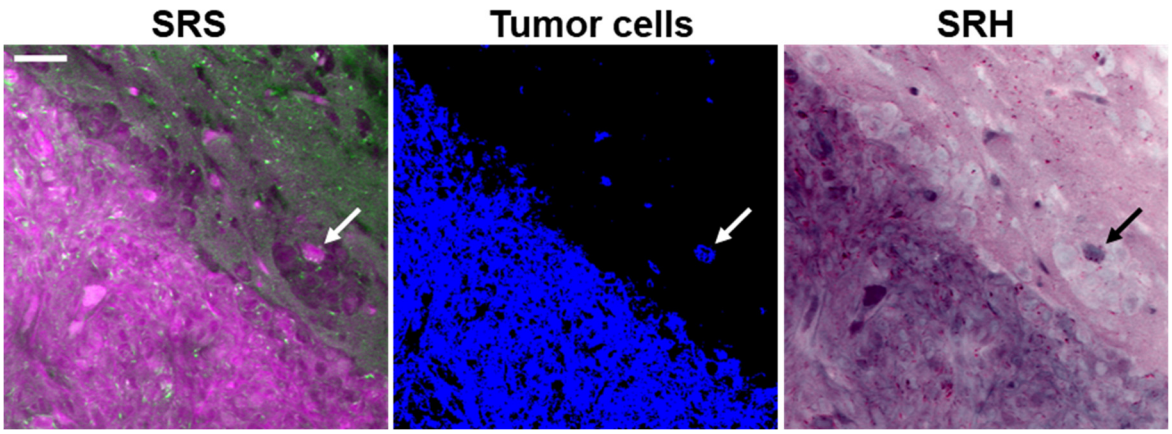

Fig. S16. Stimulated Raman histology (10) confirms tumor margins and infiltrating tumor cells identified by volumetric phasor analysis. The arrow indicates an infiltrating tumor cell. Left, SRS image. Middle, tumor cells identified by volumetric phasor analysis. Right, image of stimulated Raman histology. Scale bar: 50 μm.

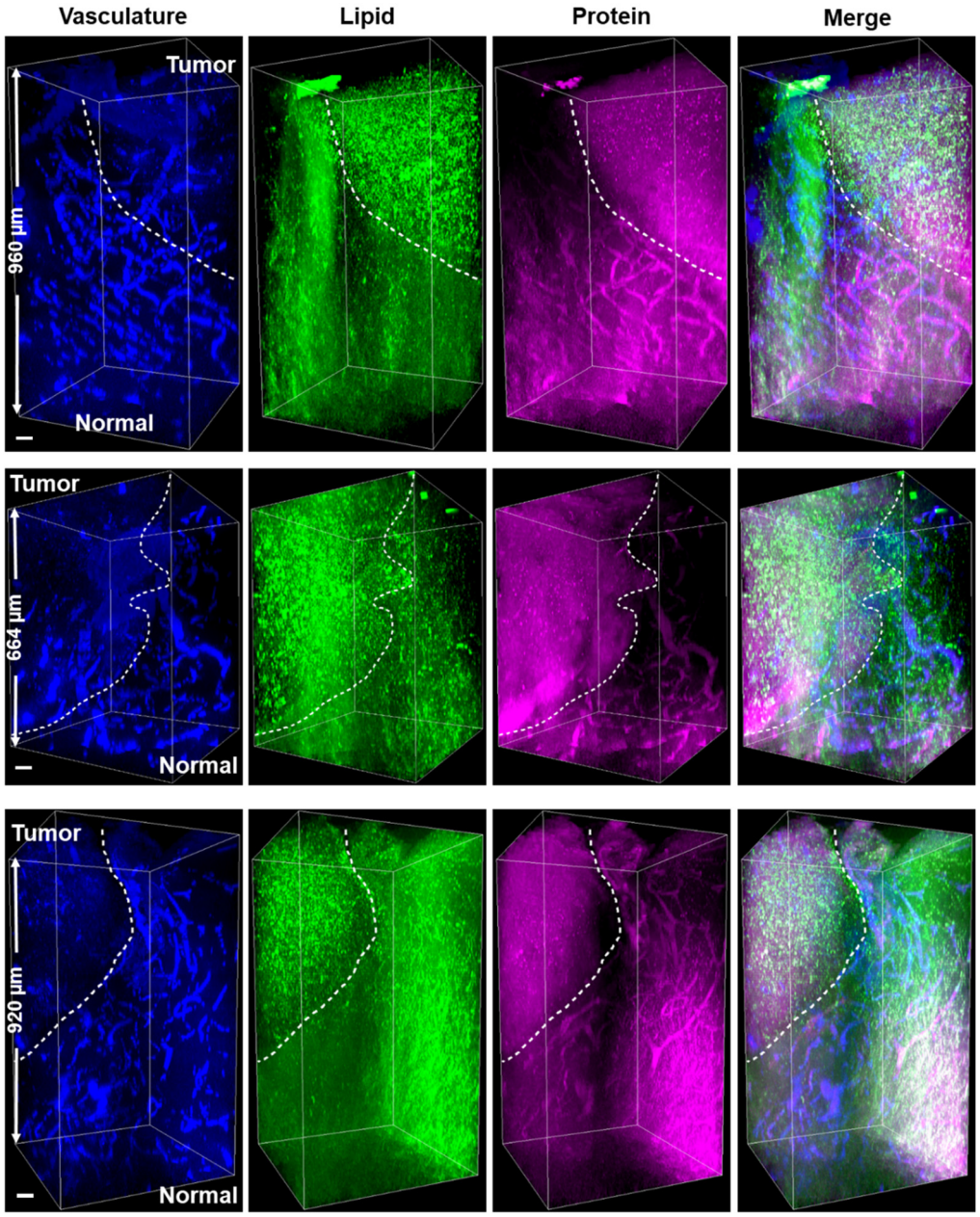

Fig. S17. Correlative two-photon fluorescence and SRS imaging of brain glioblastoma. Volume-rendered images of vasculature (two-photon autofluorescence, blue), lipids (SRS, green), proteins (SRS, magenta), and the merge. Imaging depths are labeled at the left of the autofluorscence images. White dash lines delineate the boundaries between tumor and normal tissues. Scale bars: 50 µm.

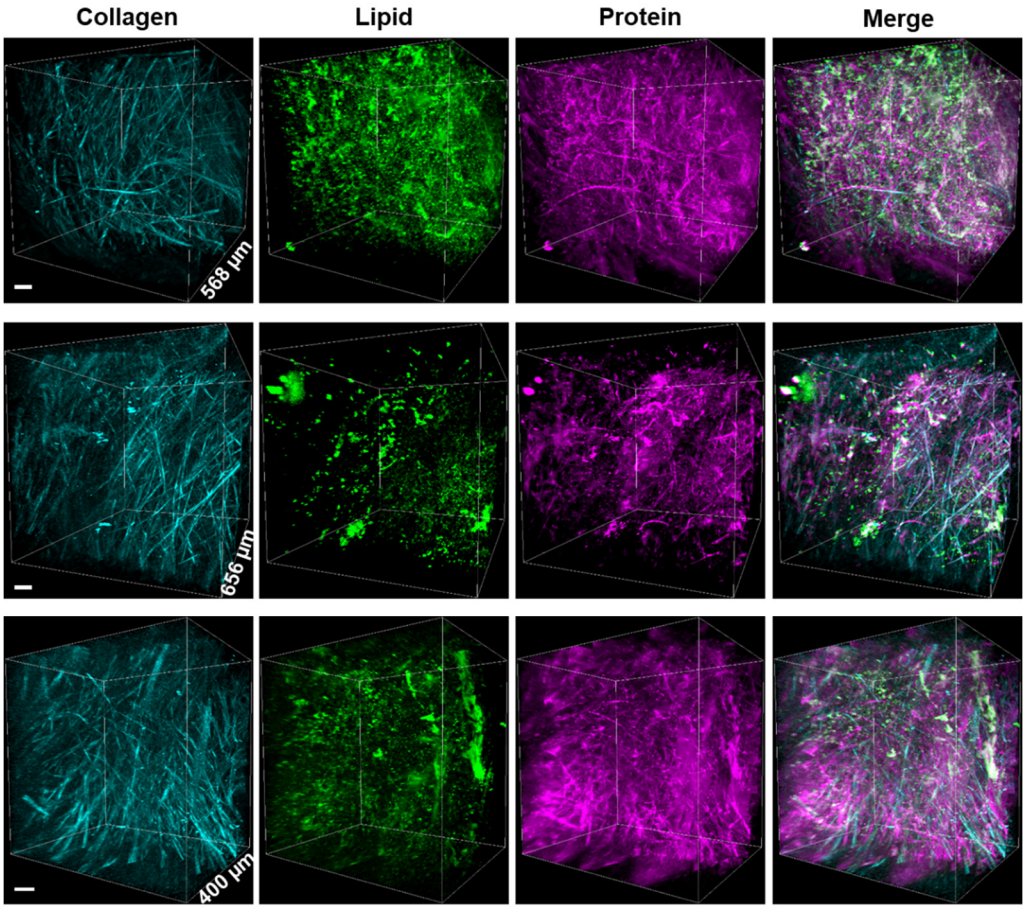

Fig. S18. Correlative second-harmonic generation and SRS imaging of subcutaneous glioblastoma. Volume-rendered images of collagen (second-harmonic generation, cyan), lipids (SRS, green), proteins (SRS, magenta), and the merge. Imaging depths are labeled at the lower right of the second-harmonic generation images. Scale bars: 50 µm.